



## Ultrasonic assisted rapid preparation of superhydrophobic stainless steel surface and its application in oil/water separation

Zongbo Zhang<sup>a,\*</sup>, Chunling Xu<sup>a</sup>, Wengang Liu<sup>a</sup>, Kai Wang<sup>a</sup>, Yunlong Rao<sup>a</sup>, Chen Jiang<sup>a</sup>, Dawei Li<sup>b</sup>, Yu Zhang<sup>a</sup>, Xin Jiang<sup>a</sup>, Xintong Chen<sup>a</sup>, Changbin Xu<sup>a</sup>

<sup>a</sup> College of Mechanical and Electrical Engineering, China University of Petroleum (East China), Qingdao 266580, PR China

<sup>b</sup> State Key Laboratory of Heavy Oil Processing, China University of Petroleum (East China), Qingdao 266580, PR China

### ARTICLE INFO

#### Keywords:

Stainless steel  
Ultrasound  
Superhydrophobic  
Ultrasonic cavitation  
Ultrasonic vibration

### ABSTRACT

The preparation of superhydrophobic (SH) surface on stainless steel by chemical etching method is challenging due to the good corrosion resistance of the material. In this work, SH surface with water contact angle (WCA) as high as 163.21° was accomplished on 304 stainless steel surface by a rapid ultrasonic-assisted chemical etching method within 7 min and a low-cost fluorine-free modification treatment. The mechanism of ultrasonic field on the etching process was explored by detecting the cavitation and oscillation energy in the reactor. It is the first time to found that the ultrasonic cavitation effect enhanced the etching process by both chemical and physical facilitation resulting in hierarchical lamellar micro-structures, “mountain-like” micro-structure clusters and “coral-reef-like” nano-scale structures on the surface. With the ultrasonic power increasing, the ultrasonic cavitation effect not only enhanced the superhydrophobicity of sample surface, but also improved the uniformity of surface wettability. The samples also showed excellent performance of oil/water separation for various organics (all separation efficiencies up to 96%) and remarkable mechanical stability.

### 1. Introduction

Superhydrophobic (SH, the static WCA greater than 150° and the sliding angle less than 10°), as one of the main surface properties of solid materials, has attracted extensive attention in the field of biology [1], chemistry [2], physics and materials science [3]. Inspired by the excellent hydrophobic properties of natural elements, such as lotus leaves [4], desert beetles [5], and the planthopper insect wing [6] etc, artificial SH surfaces have been widely explored in the past couple of decades. At present, there are various methods for preparation of SH surfaces, including chemical etching [7,8], sol-gel [9], spinning method [10,11], self-assembly method [12], electrochemical deposition [13,14], template-based method [15,16] and so on [17-19]. All the above methods indicate that both abundant surface micro-nano structures and low surface energy are vital for the preparation of SH surface. In recent years, the materials used as SH substrates are becoming more and more diversified, among which metal materials have been particularly concerned on account of their excellent mechanical properties and wide application fields [20,21].

Among the common metal materials, stainless steel is extensively

employed in the construction industry [22], aerospace field [23], medical equipment [24] and offshore operation due to its favorable corrosion resistance and excellent mechanical properties [25,26]. Just because of this good corrosion resisting property, it is fairly difficult to form abundant microcosmic morphology on the stainless steel surfaces. Therefore, many different attempts have been made to prepare SH surfaces on stainless steel over the last few decades. Vidal et al. [9] exploited sol-gel method, taking tetraethoxysilane (TEOS) and methyltriethoxysilane (MTES) as precursors to obtain the SH surface with an average WCA of 149° on the stainless steel surface. Wang et al. [27] proposed a scanning electrodeposition method to form SH nickel layer onto stainless steel surface, in which two complex solutions and tedious deposition steps were employed to obtain SH surface with WCA of 152.3°. Wu et al. [28] took advantage of a femtosecond laser for microstructure processing, after which modified the surface with silane reagent (Trichloro (1H, 1H, 2H, 2H-perfluorooctyl) silane to get a WCA of 166.3° on stainless steel surface. Although high WCAs could be obtained by this method, it was actually difficult to achieve large-scale production on account of its expensive equipment and harsh processing conditions. In general, the majority of the above methods to achieve

\* Corresponding author.

E-mail address: [zzb001\\_0@163.com](mailto:zzb001_0@163.com) (Z. Zhang).

<https://doi.org/10.1016/j.ultsonch.2021.105848>

Received 7 October 2021; Received in revised form 17 November 2021; Accepted 24 November 2021

Available online 26 November 2021

1350-4177/© 2021 The Author(s).

Published by Elsevier B.V. This is an open access article under the CC BY-NC-ND license

(<http://creativecommons.org/licenses/by-nc-nd/4.0/>).

SH stainless steel surfaces either have the disadvantage of expensive equipment or time-consuming, which hinders mass production and industrial application.

Although the corrosion resisting property of stainless steel makes it challenging to accomplish hierarchical micro-nano structure, many attempts [29,30] still focus on chemical etching method for potential low-cost mass production of SH stainless steel surfaces in recent years, due to its advantages of facile, high-efficiency and low-cost. Zhang et al. [7] etched the stainless steel surface with  $\text{FeCl}_3$  ethanol solution as the etchant for 60 min and then modified with nutmeg acid ethanol to prepare the SH stainless steel surface with WCA of  $151.6^\circ$ . Zhang et al. [31] proposed a simple wet chemical etching method to prepare the SH surface, which was chemically etched with HCl solution for 20 min and modified with perfluorinated reagent to obtain the SH surface with WCA of  $152^\circ$ . Liu et al. [32] etched stainless steel surfaces with a mixed solution composed of  $\text{FeCl}_3$ , HCl and  $\text{H}_2\text{O}_2$  for 20 min and then modified with DTS ( $\text{CH}_3(\text{CH}_2)_{11}\text{Si}(\text{OCH}_3)_3$ ) and Toluene ( $\text{C}_6\text{H}_5\text{CH}_3$ ) mixed solution to obtain the micro-nano hierarchical structure with a WCA of  $158.3 \pm 2.8^\circ$ . Our group [33] proposed a novel chemical etching method which involving  $\text{SiO}_2$ -assisted HF etching processing for 20 min. In this method, intermediate species ( $\text{H}_2\text{SiF}_6$ ) were formed to greatly enhance the corrosion process of stainless steel so as to obtain abundant micro-nano hierarchical structures on the surfaces. Even though the surfaces employed by this method were modified with Stearic acid whose price is 2–13 times lower than the fluorine modifier, the SH 304 stainless steel surfaces still achieved a static WCA of  $162.45^\circ$ . Therefore, this method has shown great advantages in not only corrosion efficiency, modifier cost but also hydrophobic properties. Although the etching time of around 20 min is relatively short for the preparation of SH stainless steel surfaces by chemical etching method compared with that in the current literatures, it is still a significant obstacle to the further improvement of production efficiency for mass production.

In this paper, we proposed an innovative strategy of ultrasonic-assisted chemical etching to further improve the above etching method. It is found that the WCA of  $163.21^\circ$  can be accomplished with the etching time of only 7 min, which indicates that ultrasonic field significantly promotes the etching process. The relationship between the WCAs and cavitation energy or non-cavitation energy was analyzed, which revealed the promotion mechanism of ultrasonic on the etching process. The results indicated that cavitation energy played a major role in the change of WCA and their variation tendency was approximately uniform. By observing the energy distribution cloud images of the cross sections, it is found that the uniformity of cavitation energy also had an obvious influence on the wettability of the stainless steel surfaces. Moreover, the application of the samples in oil–water separation was also studied, including permeation flux and separation efficiency. The results showed that the proposed simple and time-saving method was promising for the mass production of superhydrophobic stainless steel and its industrial application.

## 2. Experimental procedure

### 2.1. Preparation and characterization of superhydrophobic 304 stainless steel surfaces

The austenite stainless steel sheets with the size of  $20 \text{ mm} \times 20 \text{ mm} \times 5 \text{ mm}$  were polished with SiC paper from 800 to 2000 grades, and then cleaned by anhydrous ethanol and deionized (DI) water sequentially with ultrasonic for 5 min. After being held at  $90^\circ\text{C}$  for 20 min in an oven and dried, the sample was immersed into the etching solution of Hydrofluoric acid (HF, 40 wt%) solution and Silica powder ( $\text{SiO}_2$ , the average diameter is less than  $0.075 \text{ }\mu\text{m}$ ) (6.1 wt%, the optimal concentration) at room temperature ( $25^\circ\text{C}$ ). Two groups of comparative tests were carried out here: (1) The stainless steel substrates were etched for 5 min with the input power of ultrasound ranged from 120 to 300 W with ultrasonic cleaning machine (SB-5200 DTD, China, frequency of 20

kHz). (2) The samples were etched in etching solution for different etching times ranging from 3 min to 9 min with interval of 2 min, while the input power of the ultrasonic equipment was maintained at 300 W. Then, the samples were cleaned by ultrasonic for 5 min with anhydrous ethanol and DI water to remove the reaction residues and dried in atmosphere. Thereafter, the samples were immersed into stearic acid ethanol solution ( $(\text{C}_{18}\text{H}_{36}\text{O}_2)$ , 0.05 mol/L) for 1 h at room temperature. Finally, the samples were washed and dried with temperature of  $100^\circ\text{C}$  for 1 h. All chemicals used in the present experiments were of analytical grade and used without further purification.

The WCAs of the samples were measured by a contact angle measuring instrument (SL200B, USA, KINO). The samples were measured by dripping  $3 \text{ }\mu\text{L}$  droplets of DI water at five different locations on the substrate surface and the average value was taken as the final WCA. The microstructures of the surface were characterized with field emission scanning electron microscopy (FE-SEM) (JSM-7200F, Japan, JEOL).

### 2.2. Sound field measurement in sonochemical reactor

The experimental apparatus for the measurement of sound pressure is shown in Fig. 1. The acoustic signal in the reactor was measured by hydrophone, and then the intensity of cavitation field in the reactor was quantitatively evaluated by further analyzing the collected cavitation noise spectrum information. The hydrophone (TC4034; RESON A/S, Slangerup, Denmark) was fixed using a self-developed 3D dimensional positioning system holder [34]. The digital oscilloscope (DS2102, RIGOL, China) recorded the acoustic signal collected from the hydrophone, and then a computer converted the acoustic signal to sound pressure signal by a self-developed software. An example of sound pressure spectrum as shown in Fig.S1. The etching reactor was placed in the ultrasonic cleaning machine. The measurement points diagram and experimental diagram are shown in Fig. 2. In this experiment, the measurement range was limited to the reactor. The measurement path of the hydrophone was eight concentric circles with different radius as shown in Fig. 2(a). Actually, the measurement points on each circumference were 12 points.

In general, the ultrasonic energy was divided into cavitation energy and non-cavitation (vibration) energy [35]. The cavitation energy is evaluated by the broadband integrated pressure (BIP), which is mainly derived from the radiation force and acoustic micro-streaming produced by the fluctuation of cavitation bubbles, and the shock wave emitted from the collapse of cavitation bubbles [36–38]. The non-cavitation energy is evaluated by the fundamental wave pressure (FWP), which is mainly derived from the ultrasonic vibration [34,39].

### 2.3. Experiment and characterization of superhydrophobic materials in oil/water separation

As shown in Fig. 3, a simple device made of the obtained superhydrophobic stainless steel meshes had been designed for oil/water separation. Considering that the superhydrophobic 304 stainless steel meshes were applied to separate oil/water mixtures, the samples (300#) with ultrasonic power of 300 W and etching time of 7 min were chosen. Here, we chose various organics, such as n-hexane, crude oil, petroleum ether, kerosene, dichloromethane to constitute the oil/water mixtures (volume ratio is 1:1). When the oil/water mixtures were tardily poured onto the stainless steel meshes prewetted with oil, the oil penetrated the meshes and flowed down the beaker underneath, whereas the water retained on the surface of the 304 SS meshes, the separation process was shown in Video.S1. The separation process is driven only by gravity and the oil/water separation mechanism was shown in attachment C. Moreover, the advantage of this device is that it could measure the pressure resistance of mesh accurately without any deformation of mesh surface and damage of the SH surface [40].

The properties of superhydrophobic stainless steel meshes are char-

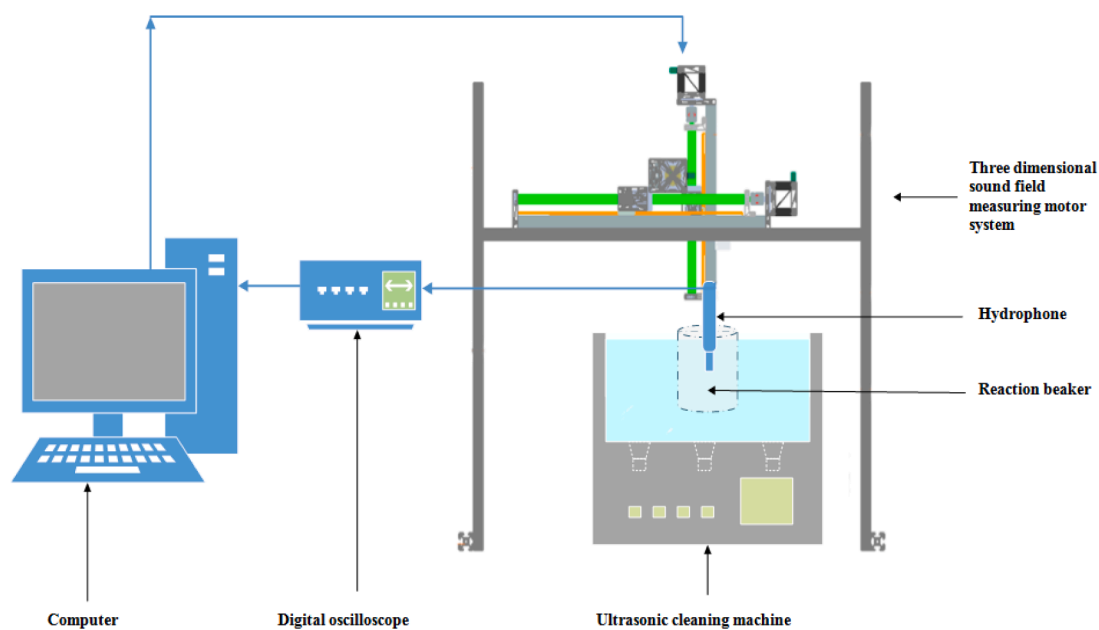


Fig. 1. Diagram of hydrophone experiment.

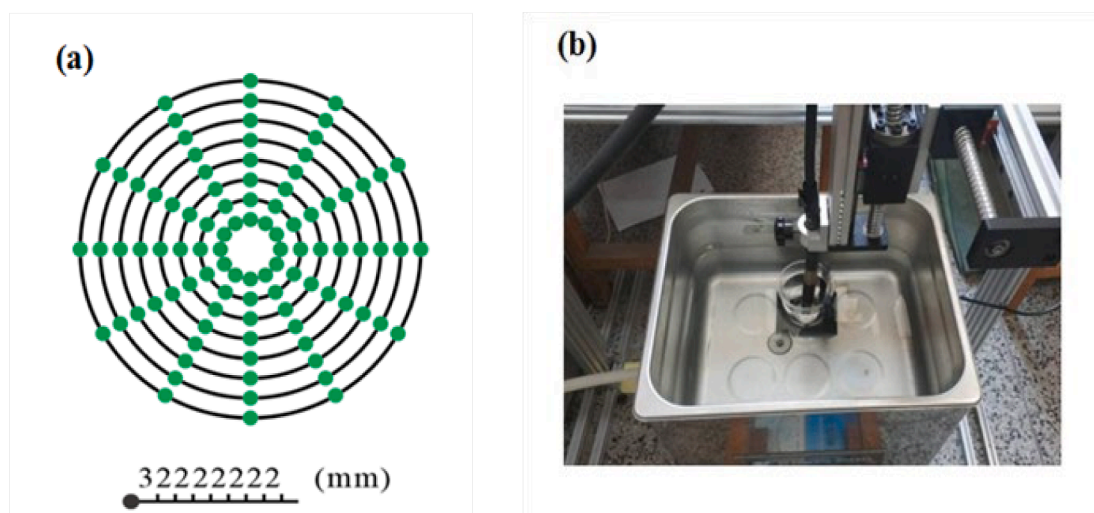


Fig. 2. Experiment of hydrophone measurement: (a) the measurement points diagram, (b) the hydrophone measurement experimental diagram.

acterized in three aspects: pressure resistance, separation efficiency and permeability flux. Therein, the maximum height of water was obtained by pouring water onto the meshes until water penetrating the meshes as shown in Fig.S2 and then the water pressure resistance ( $P_0$ ) can be calculated as Eq. (1):

$$P_0 = \rho g h_{\max} \quad (1)$$

Where  $\rho$  represents the density of water,  $g$  is the acceleration of gravity, and  $h_{\max}$  indicates the maximum height of water that the mesh can support without penetration. In addition, the separation efficiency of the functional stainless steel meshes was investigated, which can be quantitatively calculated by means of the following Eq. (2):

$$\eta = \frac{V_1}{V_0} \times 100\% \quad (2)$$

Where  $V_0$  is the original oil volume in oil/water mixtures and  $V_1$  donates the volume of harvested oil after separation. Finally, the permeability flux of the SH stainless steel mesh can be calculated

according to Eq. (3) below:

$$Flux = V / (S \times t) \quad (3)$$

Where  $V$  is the volume of captured oil,  $S$  is the area of the mesh, and  $t$  represents the permeation time of oils. For the penetration flux of pure oil, we recorded the time of 50 ml pure oil fully penetrating the stainless steel meshes. Analogously, 50 ml of oil/water mixture (volume ratio = 1:1) was poured onto the meshes and the time for oil to fully penetrate the meshes was recorded.

### 3. Results and discussions

#### 3.1. Mechanism of ultrasonic field on etching process

Fig. 4 shows the relationship between the ultrasonic energy and the WCAs of 304 SS surface under different input powers (120–300 W) at room temperature. The ultrasonic energy in the reactor was separated into cavitation energy and non-cavitation energy as mentioned part 2.2

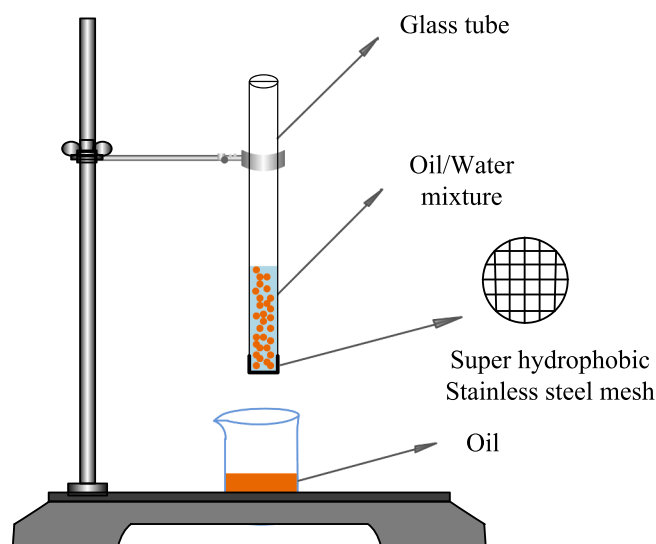
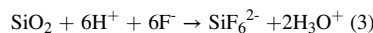
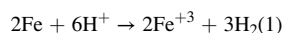


Fig. 3. Image and schematic illustration of oil–water separation apparatus.

and attachment A. The results illustrated that the variation tendency of WCAs coincided with that of cavitation energy, which gradually increased with the enhancement of cavitation energy. The increase of cavitation energy meant more cavitation-bubble-collapsions occur resulting in transient high temperature (up to 5000 K) [41], ultra-high pressure (about  $5.05 \times 10^8$  Pa) [42] and super strong micro-jet (the rate up to 400 Km/h) [43], which can significantly promote the etching process in the following ways:

- (1) Chemical facilitation, the high temperature and pressure produced by the bubble collapse can generate more radical  $H^+$  by dissociating the HF solution. The increase of  $H^+$  not only accelerated the etching reaction of 304SS as shown in Eq (1)–(2), but also promoted the chemical reaction with  $SiO_2$  as shown in Eq (3). The formation of Hexafluorosilicic acid ( $H_2SiF_6$ ) can further facilitate the corrosion of Fe element [33].



- (2) Physics promotions, smaller cavitation bubbles generated at higher pressure could penetrate into the cavities and the micro-cracks of the solid phase and destroyed them [44]. Then, strong micro-jet generated by the bubble collapse can lead to severe local micro turbulence and enhance mass transfer, which resulted in the exfoliation of unstable particles.

On the contrary, the tendency of non-cavitation energy was quite different, which rose first and then decreased, with the maximum non-cavitation of 56.24 kPa·kHz reached at input power of 180 W, as shown in Fig. 4. The decrease of non-cavitation energy during the input power above 180 W mainly resulted from the growing number of cavitation bubbles hindering the propagation of ultrasonic oscillation. More specifically, the WCAs with ultrasonic power of 120 W and 300 W were notably different but the non-cavitation energy of these two cases were almost the same. It was implied that non-cavitation energy has no obvious correlation with the etching process.

In summary, the ultrasonic cavitation effect dominated the enhancement of corrosion process, however the oscillation induced by ultrasound not apparently effected the corrosion.

To reveal the influence of ultrasonic on the surface morphology, SEM micrograph patterns of the samples with different input power (120–300 W) are presented in Fig. 5. Compared with the no-ultrasonic-assisted sample as shown in Fig. 5(a), the ultrasonic-assisted samples showed obviously more abundant lamellar micron-scale structures and “mountain-like” microstructure clusters on both of which the “coral-reef-like” nano-scale structures uniformly covered as shown in Fig. 5(b)–(e). After surface modification these hierarchical micro-nano structures can easily result in tiny air bags to prevent water penetration, which was governed by Cassie model as shown in Fig. 6(b). However, despite the surface of samples without ultrasound was slightly etched resulting in some lamellar micron structures, the depth of these structures were obviously shallower and the distribution was more irregular, which

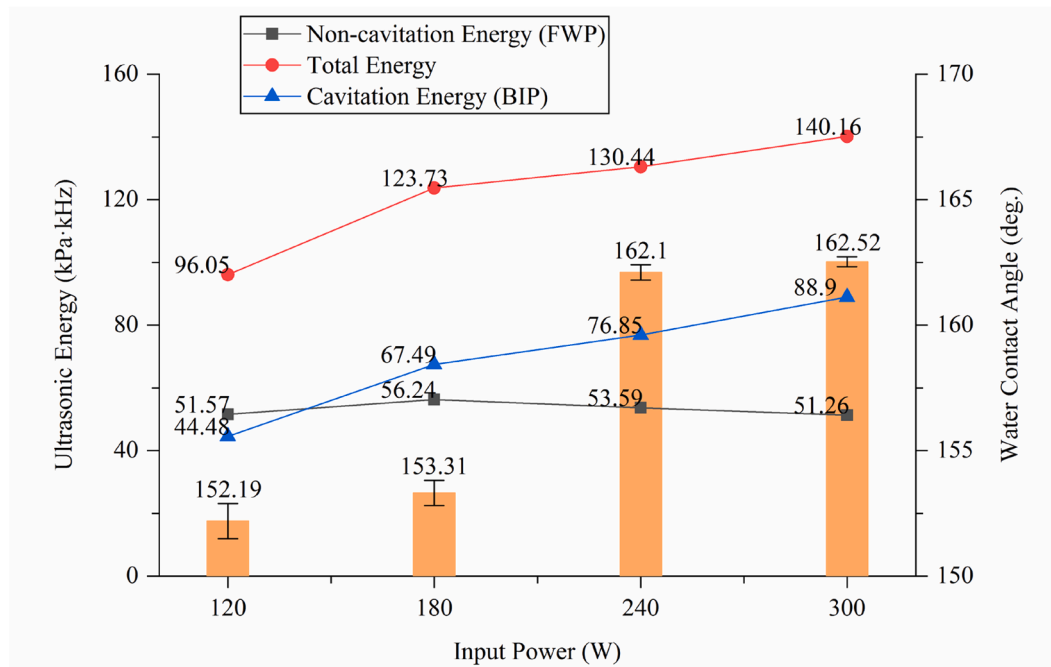


Fig. 4. The relation between ultrasonic energy and water contact angle at different input power.

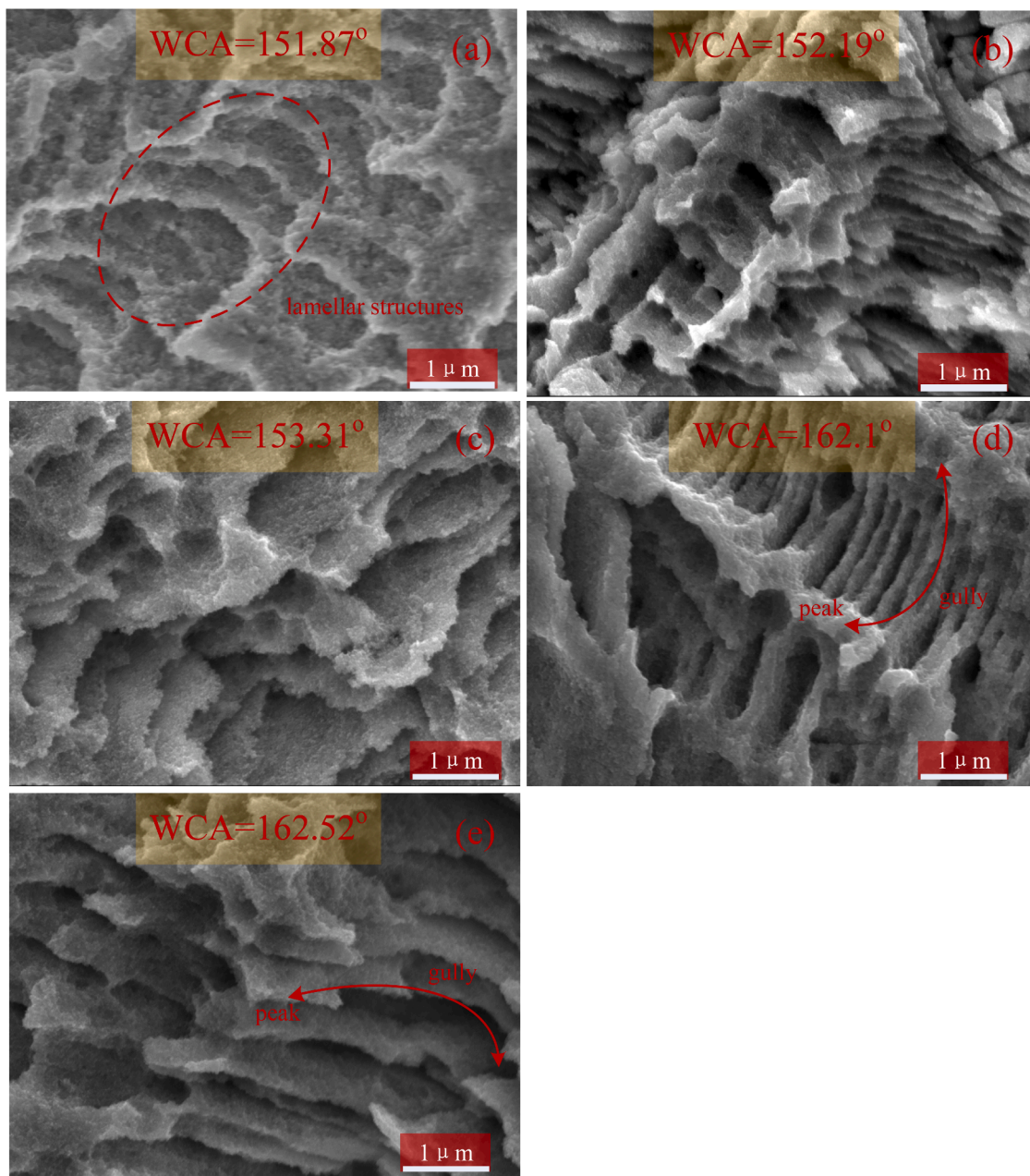


Fig. 5. SEM images of SH surfaces prepared at different ultrasonic powers: (a) without ultrasonic, (b) 40%, (c) 60%, (d) 80%, (e) 100%.

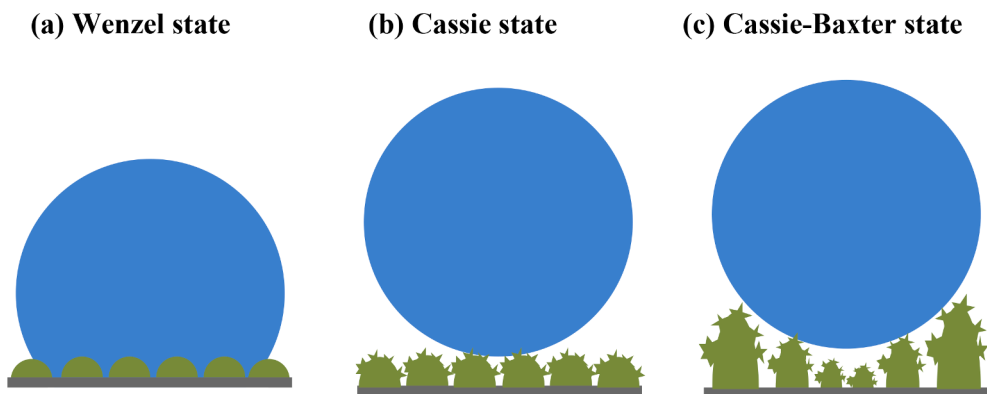


Fig. 6. Schematic illustrations of the hydrophobic state of the samples. (a) after HF etching and modification without ultrasonic, (b) after ultrasonic-assisted HF etching and modification, (c) after 7 min of ultrasonic-assisted HF etching and modification.

caused the contact situation with water accord with Wenzel model as shown in Fig. 6(a). The results indicated that the ultrasonic field significantly stimulated the development of the microstructure on 304 SS surface during the etching process.

In addition, the SEM images also illustrated that with the increase of input power, the micron-scale structures deepened obviously, and their distribution was more regular. The lamellar structure interconnected with each other to form “mountain-like” microstructure clusters as shown in Fig. 5(d)-(e). This was mainly attributed to that the enhancement of the cavitation energy with the increase of input power not only intensified the reaction between the reaction solution and the 304SS substrate surface, but also promoted the strong micro-jet to remove the detached particles from the micro-cracks efficiently. Consequently, all the “mountain-like” microstructure clusters, lamellar microstructures as well as the “coral-reef-like” nano-scale structures resulted in a very high WCA of more than  $162^\circ$ , which was governed by Cassie-Baxter model as shown in Fig. 6(c).

It is surprising to notice that the error magnitude of WCAs decreases obviously with the increase of ultrasonic power as shown in Fig. 4. This phenomenon indicated that with the increase of input power, the enhancement of ultrasonic cavitation effect significantly improved the uniformity of the formed microstructure.

In order to figure out the mechanism of this phenomenon, the uniformity of ultrasonic cavitation energy distribution in the reactor under different input powers were measured as shown in Fig. 7, in which red represented the high energy area and blue signified the low energy area. In this paper, MATLAB was employed for the signal processing and visualization. It is worth noting that we had carried out logarithmic (lg) operation on the energy values in order to narrow the gap between the energy values which resulted in observing the changes of the energy of the sound field more clearly. All contours showed that the cavitation energy at the center part of the cross section was high, so this part was chosen as the etching area. As shown in Fig. 7, there was no center of energy distribution for following two reasons. First, the sound field signal measuring device was a self-made equipment. Its planned route is rectangular, while the energy distribution diagram in this paper is circular, so it is difficult for the sensor to reach the central measuring position. Besides, in the process of measuring sound field signals, in order

to more clearly reflect the energy distribution of sound field, “interp2” interpolation function was used to interpolate between the energy at the measured positions. The energy near the center could not be interpolated, resulting in the energy at the very center point was hard to be measured according to the planned measurement path (as shown in Fig. 2(a)). In general, central energy was higher and more uniform, which was treated as high energy area. The results also showed that the distribution of the cavitation energy was greatly un-uniform when the input power was 120 W, as shown in Fig. 7(a). However, with the increase of input power, not only the proportion of high energy area increased which stimulated the increase of WCAs, but also uniformity of the cavitation energy was obviously improved, which contributed to the improvement of the corrosion uniformity.

### 3.2. Effect of ultrasonic time on wettability

In order to reveal the effect of ultrasonic time on the contact angle, the four samples were prepared by setting the ultrasonic input power of 300 W with different etching time ranging from 3 min to 9 min as mentioned in Part 2.1.

The results in Fig. 8 illustrated that all the obtained WCAs of the samples were higher than  $157^\circ$ , suggesting that the ultrasonic field successfully enhanced the superhydrophobicity on the surface of stainless steel even the etching time was as short as 3 min. Especially, with the ultrasonic time increasing, the WCAs first increased reaching the maximum value of  $163.21^\circ$  under the ultrasonic time of 7 min and then decreased. The enhancement of contact angles attributed to the increase of ultrasonic-assisted etching time, which stimulated the formation of the “mountain-like” micron-scale structures as shown in Fig. 9. Obviously, the “mountain-like” microstructures gradually changed from flat-top (as shown in Fig. 9(a)) to pinnacle (as shown in Fig. 9(b) and (c)). However, with further increase of etching time, the “mountain-like” microstructures were over-etched and then became flat-top again as shown in Fig. 9(d). Analogously, Fig. 10 schematically illustrated the detailed changing process of the “mountain-like” microstructures. It was supposed that the corrosion rate for any direction of the microstructures was the same. As the etching time increased from 3 min to 7 min, the top of the “mountain-like” microstructures got sharper and the gully got

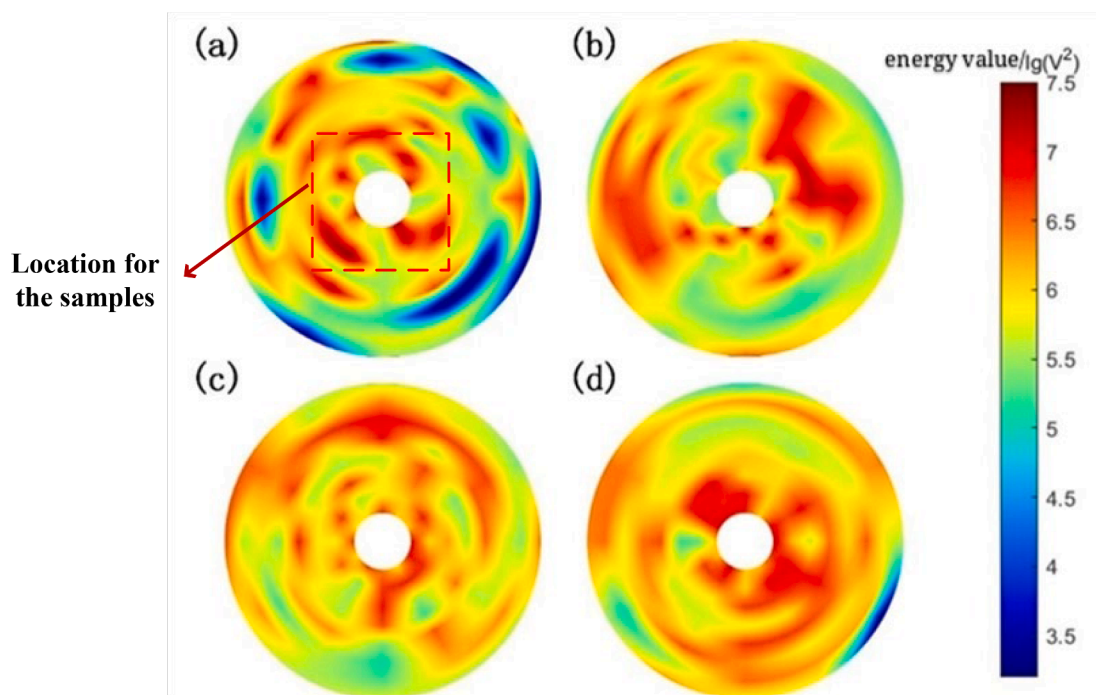


Fig. 7. Cross section energy distribution of ultrasonic chemical reaction field: (a) 40%, (b) 60%, (c) 80%, (d) 100%.

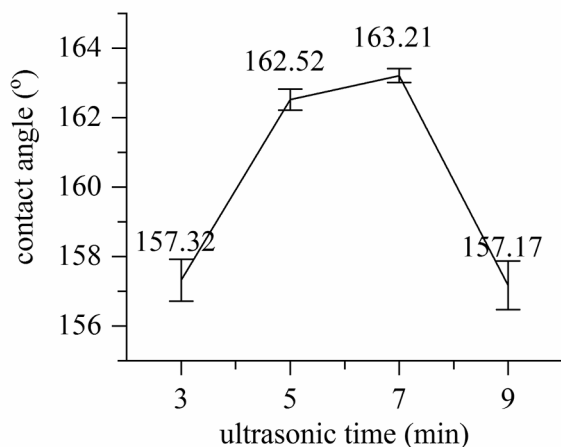


Fig. 8. Relationship between static WCAs and ultrasonic time.

deeper as shown in Fig. 10(L<sub>2</sub>-L<sub>4</sub>), which could prompt to form thicker air cushions between solid and droplets. Nevertheless, when the etching time prolonged from 7 min to 9 min, the etching rate of the very sharp peaks was higher than that of the gully, which was because the previously formed peaks were extremely weak and easily to be destroyed by over-corrosion and cavitation effect, resulting in flat-top “mountain-like” with relatively low height as shown in Fig. 10 L5. The above-mentioned change in the “peak” structure showed the gas storage capacity of the microstructure on the solid surface, which is consistent with the change trend of the surface wettability shown in Fig. 8.

It is apparent that there is a specific hierarchical surface structures required for a high contact angle of 163.21° under the ultrasonic time of 7 min. Compared with the process without ultrasonic-assisted corrosion

(the optimal etching time was 20 min), not only the preparation time shortened by more than 2 times, but also the contact angles slightly improved (the WCA of obtained surface without ultrasonic-assisted etching process was 162.45°) [33]. This simple and time-saving method is especially vital for the mass production of superhydrophobic stainless steel materials.

### 3.3. Application of SH stainless steel in separation of oil/water mixtures

In order to explore the application of the above superhydrophobic stainless steel in oil/water separation, the performance of meshes was characterized by pressure resistance, separation efficiency and oil flux for various organics (n-hexane, crude oil, petroleum ether, kerosene, dichloromethane).

The water pressure resistance presents the maximum height ( $h_{max}$ ) of liquid that the meshes could support [45]. The experimental result showed that the maximum intercepted water height was 27.3 cm (as shown in attachment C), which was higher than that of most of previous reports (Table 1). Superhydrophobic stainless steel mesh with high pressure resistance could withstand greater external pressure and separate oil/water mixtures effectively, which was significant for the practical application.

The separation efficiencies for various organics ranged from 96.8% to 98.4% as shown in Fig. 11. The high values demonstrated that the as-prepared stainless steel mesh could separate various oil/water mixtures with competent efficiencies. In addition, the durability of the mesh was investigated by taking the kerosene/water mixtures as an example of which the separation efficiency remained more than 97% after 10 cycles of separation (as shown in S1). These results indicated that the as-prepared superhydrophobic stainless steel mesh displayed stable recyclability. Additionally, the flux of oil samples is an important indicator to show the separation rate in the industrial oil/water separation application [50]. Owing to the oleophilicity of the as-prepared mesh,

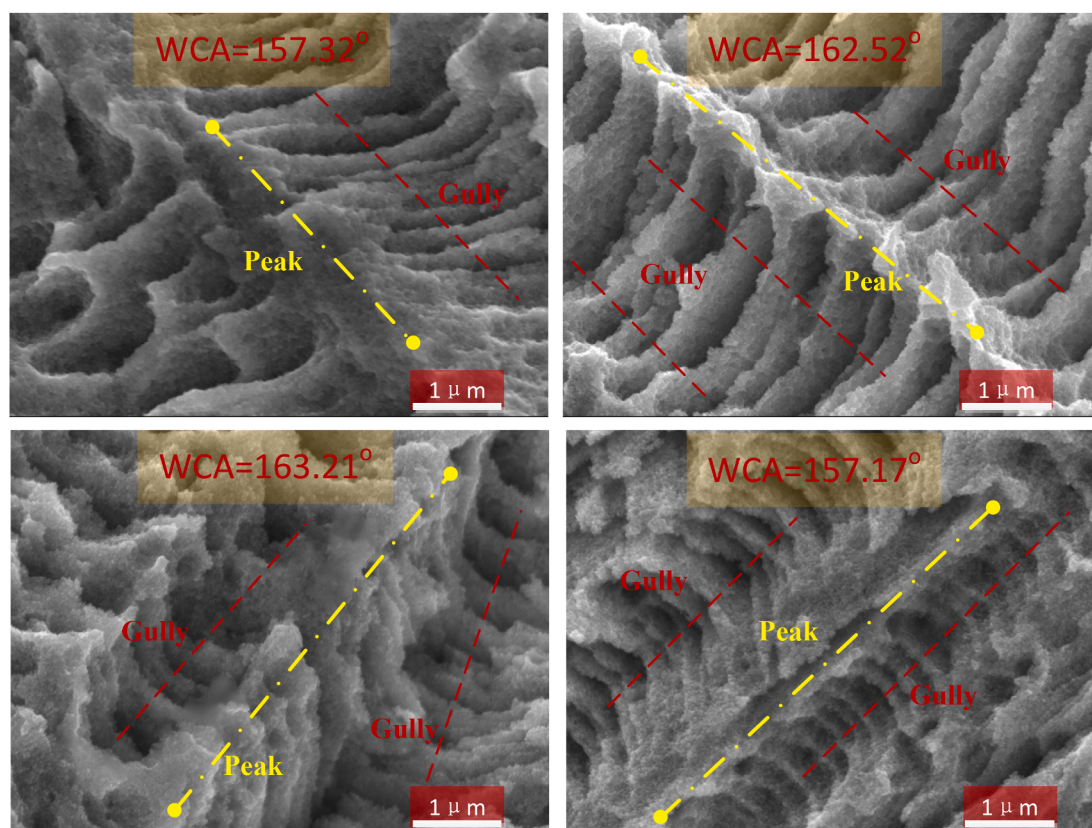
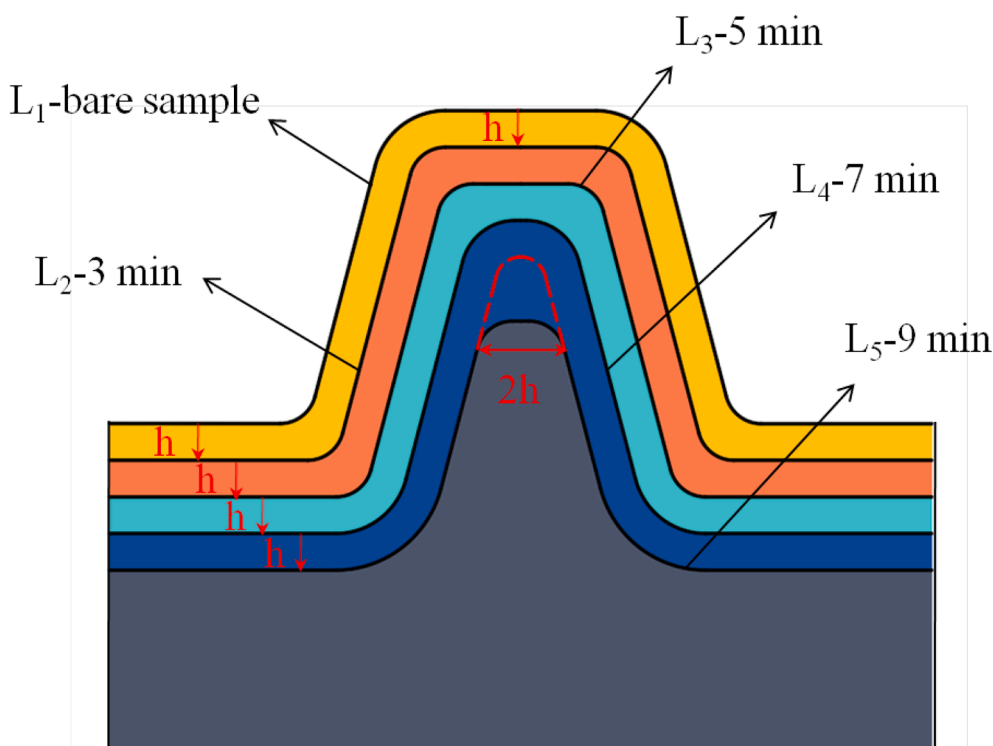


Fig. 9. SEM images of SH surfaces prepared under different ultrasound times: (a) 3 min, (b) 5 min, (c) 7 min, (d) 9 min.



**Fig. 10.** Schematic diagram of original structure (a) and microstructure change with the increase of ultrasonic-assisted etching time: (b) 3 min, (c) 5 min, (d) 7 min, (e) 9 min.

**Table 1**  
Pressure resistance by different methods.

Materials	Methods	Pressure (kPa)	References
304 stainless steel	Chemical etching method	2.68	This work
Zeolite-coated mesh	Secondary growth method	0.96	[46]
Phenol-formaldehyde resin	Spray method	0.951	[47]
Stainless steel	Electrophoretic deposition method	2.29	[48]
Copper mesh	Selective electrodeposition method	~1.3	[49]

500 ml oil fully passed through the stainless steel mesh within a few seconds with only gravity-driven force [51], and all oil flux were larger than  $6.68 \text{ L m}^{-2} \text{ s}^{-1}$  as shown in Fig. 11. Due to the excellent corrosion resistance of stainless steel and its good application prospect in the field of oil/water separation, many studies on the preparation of superhydrophobic stainless steel surface and its application on oil/water separation have been reported. Fig. 12 showed the separation efficiencies of superhydrophobic stainless steel surfaces obtained from different methods [48,52-54]. It was indicated that the separation efficiency of the as-prepared samples ranked among the highest values reported before. Besides, the WCA ( $163.21^\circ$ ) of samples could be accomplished with the etching time of only 7 min, and low-cost fluorine-free reagents for modification, which was promising in large-scale industrial production. However, the other methods mentioned in Fig. 12 still existed some inadequacy on preparation time, reagent or equipment cost, which hindered the industrial application of superhydrophobic stainless steel mesh for oil/water separation. Therefore, the high separation efficiency and flux indicated that the as-prepared stainless steel mesh was promising in separation of oil/water owing to the superior surface wettability and the excellent corrosion resistance of the substrate.

In addition, in the industrial application of oil/water separation, the

micro/nano structures and wettability on the surface of superhydrophobic/superoleophilic materials are easily destroyed in harsh environments [55]. Hence, the mechanical stability was investigated by sandpaper abrasion test. The as-prepared meshes were dragged along sandpaper (1500 grits) using 2 N weight for a cycle (20 cm) as shown in Fig. 13(a). The relationship between WCAs and abrasion cycles suggested that the WCAs gradually decreased and tended to hold steady with the increase of abrasion cycles and even after 10 abrasion cycles the mesh was still superhydrophobic (WCA was  $152.25^\circ$ ) as shown in Fig. 13 (b), indicating that the as-prepared stainless steel mesh maintained excellent mechanical durability.

#### 4. Conclusions

In this paper, an efficient method of ultrasonic-assisted chemical etching for preparing superhydrophobic surface on stainless steel was proposed. The mechanism of ultrasound promoting the etching process was studied. It is the first time to demonstrate that the ultrasonic cavitation effect enhanced the etching process from both physical and chemical ways. The local high-temperature and high-pressure produced by cavitation stimulated the etching solution dissociating more  $\text{H}^+$  to positively promote the progress of etching reaction. The generated strong micro-jet and other accompanying phenomena removed the residual reactants on the surface to ensure the etching solution and the sample surface fully contact. The increase of ultrasonic power led to the enhancement of ultrasonic cavitation effect, which not only enhanced the surface superhydrophobicity, but also improved the uniformity of surface wettability. Further research showed that the time of ultrasonic action significantly affected the size and morphology of the micron structures to influence the WCAs. The results indicated that the optimal WCA ( $163.21^\circ$ ) can be obtained within only etching 7 min. In addition, the as-prepared sample displayed high pressure resistance (up to 2.68 kPa), separation efficiency (all up to 96.8%) and oil flux (up to  $6.68 \text{ L m}^{-2} \text{ s}^{-1}$ ), indicating excellent oil/water separation performance.

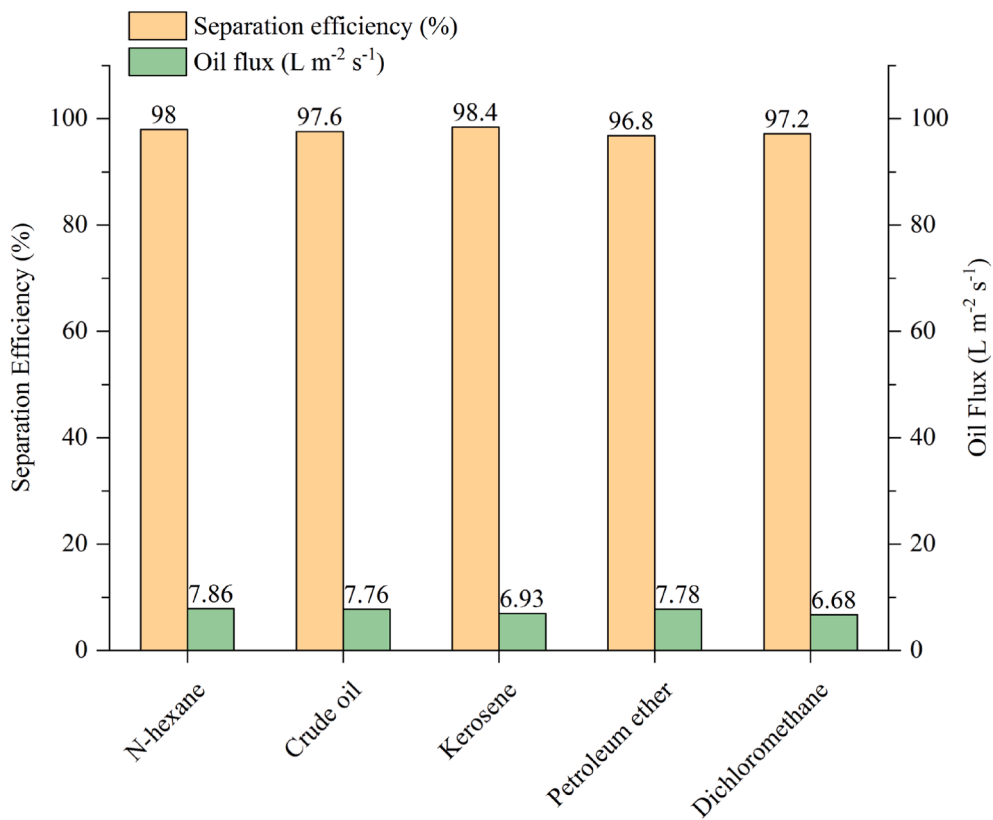


Fig. 11. Oil/water separation efficiency and oil flux of the SH stainless steel mesh for kinds of sample oils.

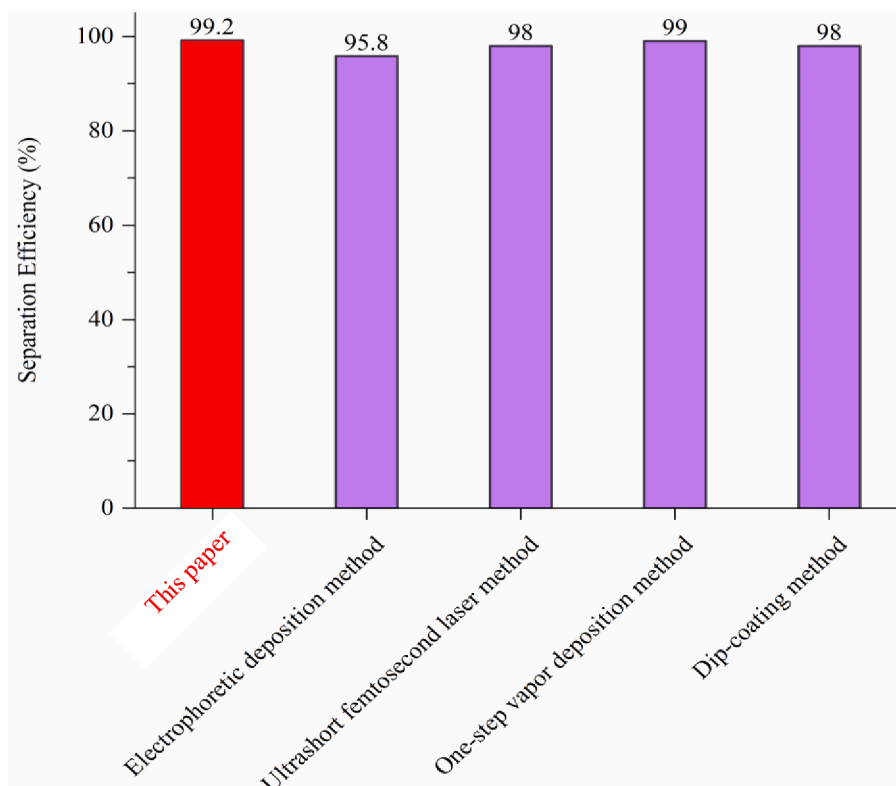


Fig. 12. Oil/water separation efficiency of the SH stainless steel mesh for kinds of methods.

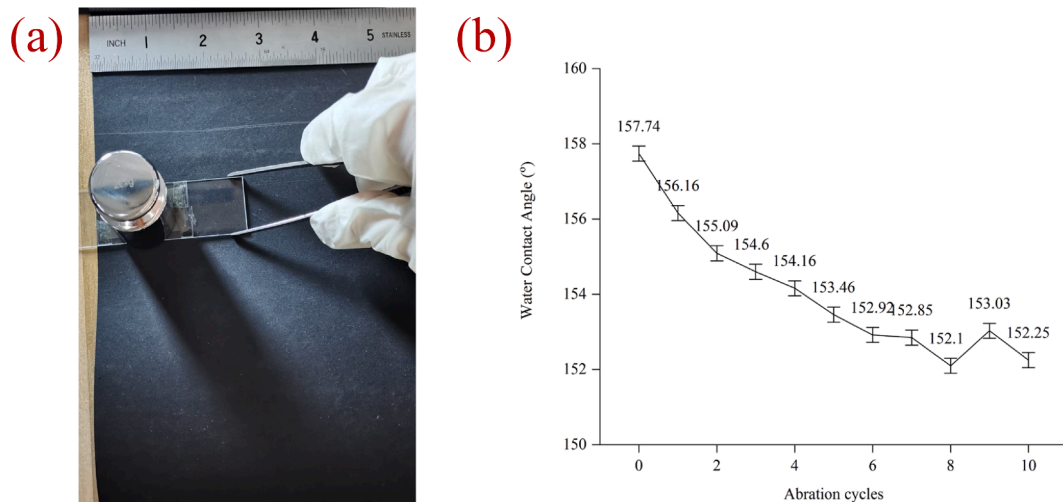


Fig. 13. The mechanical stability test: (a) Sandpaper abrasion test. (b) The WCAs after 0–10 abrasion cycle tests.

### CRedit authorship contribution statement

**Zongbo Zhang:** Conceptualization, Data curation, Writing – original draft, Writing – review & editing. **Chunling Xu:** Data curation, Formal analysis, Visualization, Writing – original draft. Other Co-Authors contributions: all co-authors have almost contributed equally.

### Declaration of Competing Interest

The authors declare that they have no known competing financial interests or personal relationships that could have appeared to influence the work reported in this paper.

### Acknowledgements

This work was supported by the National Natural Science Foundation of China 51905546 and 51205414), Key - Technology Research and Development Program of Shandong (2018GGX103034), Shandong Natural Science Foundation (ZR2017QEE006) and Fundamental Research Funds for the Central Universities (18CX02121A and 19CX02020A).

### Appendix A. Supplementary data

Supplementary data to this article can be found online at <https://doi.org/10.1016/j.ultsonch.2021.105848>.

### References

- [1] K.S. A., D. P., D. G., N. J., H. G.S., A.S. S., J. K., M. R., Mechanism, fabrication and its application in medical implants to prevent biomaterial associated infections, *J. Ind. Eng. Chem.* 92 (2020) 1–17.
- [2] B. Li, et al., One-step electrochemical deposition leading to superhydrophobic matrix for inhibiting abiotic and microbiologically influenced corrosion of Cu in seawater environment, *Colloids Surf., A* 616 (2021), 126337.
- [3] K. Liu, Y.e. Tian, L. Jiang, Bio-inspired superoleophobic and smart materials: Design, fabrication, and application, *Prog. Mater. Sci.* 58 (4) (2013) 503–564.
- [4] M. Przybylak, H. Maciejewski, A. Dutkiewicz, I. Dąbek, M. Nowicki, Fabrication of superhydrophobic cotton fabrics by a simple chemical modification, *Cellulose* 23 (3) (2016) 2185–2197.
- [5] T. Darmanin, F. Guittard, Superhydrophobic and superoleophobic properties in nature, *Materials today (Kidlington, England)* 18 (5) (2015) 273–285.
- [6] G.S. Watson, D.W. Green, B.W. Cribb, C.L. Brown, C.R. Meritt, M.J. Tobin, J. Vongsivut, M. Sun, A.-P. Liang, J.A. Watson, Insect Analogue to the Lotus Leaf: A Planthopper Wing Membrane Incorporating a Low-Adhesion, Nonwetting, Superhydrophobic, Bactericidal, and Biocompatible Surface, *ACS Appl. Mater. Interfaces* 9 (28) (2017) 24381–24392.
- [7] Z. Zhang, Y. Chen, Q. Gu, D. Chen, H. Liu, X. Li, Y. Chen, Preparation and Corrosion Resistance of 304 Super-hydrophobic Stainless-Steel Surface. IOP conference series, *Materials Science and Engineering* 493 (2019) 012057, <https://doi.org/10.1088/1757-899X/493/1/012057>.
- [8] Y. Wenxuan, Y. Yuan, L. Guoyong, Z. Bing, Y. Rongkai, The anti-icing/frosting aluminum surface with hydrangea-like micro/nano structure prepared by chemical etching, *Mater. Lett.* 226 (2018) 4–7.
- [9] K. Vidal, E. Gómez, A.M. Goitandia, A. Angulo-Ibáñez, E. Aranzabe, The Synthesis of a Superhydrophobic and Thermal Stable Silica Coating via Sol-Gel Process, *Coatings* 9 (10) (2019) 627, <https://doi.org/10.3390/coatings9100627>.
- [10] B. Ding, T. Ogawa, J. Kim, K. Fujimoto, S. Shiratori, Fabrication of a superhydrophobic nanofibrous zinc oxide film surface by electrospinning, *Thin Solid Films* 516 (9) (2008) 2495–2501.
- [11] K.-H. Cho, L.-J. Chen, Fabrication of sticky and slippery superhydrophobic surfaces via spin-coating silica nanoparticles onto flat/patterned substrates, *Nanotechnology* 22 (44) (2011) 445706, <https://doi.org/10.1088/0957-4484/22/44/445706>.
- [12] S. Dou, et al., Self-assembly of super-hydrophobic PMMA microspheres on silicon wafer as MALDI-MS chip for rapid quantification of peptides, *Sens. Actuators, B* 306 (2020), 127573.
- [13] H. Şakalak, et al., Roll-to roll initiated chemical vapor deposition of super hydrophobic thin films on large-scale flexible substrates, *Chem. Eng. Sci.* 215 (2020), 115466.
- [14] Y.i. Lin, J. Han, M. Cai, W. Liu, X. Luo, H. Zhang, M. Zhong, Durable and robust transparent superhydrophobic glass surfaces fabricated by a femtosecond laser with exceptional water repellency and thermostability, *J. Mater. Chem. A* 6 (19) (2018) 9049–9056.
- [15] J.J. Victor, D. Facchini, U. Erb, A low-cost method to produce superhydrophobic polymer surfaces, *J. Mater. Sci.* 47 (8) (2012) 3690–3697.
- [16] Q. Wang, Y. Song, L.i. Wang, J. Xiao, Fabrication of template with dual-scale structures based on glass wet etching and its application in hydrophobic surface preparation, *Micro & Nano Letters* 9 (5) (2014) 340–344.
- [17] L. Feng, Y. Zhu, J. Wang, X. Shi, One-step hydrothermal process to fabricate superhydrophobic surface on magnesium alloy with enhanced corrosion resistance and self-cleaning performance, *Appl. Surf. Sci.* 422 (2017) 566–573.
- [18] J. Feng, M.T. Tuominen, J.P. Rothstein, Hierarchical Superhydrophobic Surfaces Fabricated by Dual-Scale Electron-Beam-Lithography with Well-Ordered Secondary Nanostructures, *Advanced Functional Materials* 21 (19) (2011) 3715–3722.
- [19] D. Chu, X. Sun, Y. Hu, J.-A. Duan, Substrate-independent, switchable bubble wettability surfaces induced by ultrasonic treatment, *Soft Matter* 15 (37) (2019) 7398–7403.
- [20] Z. Yu, et al., Research on a reversible superwetting behavior and its corrosion resistance, *Appl. Surf. Sci.* 517 (2020), 146145.
- [21] X. Li, Q. Zhang, Z. Guo, T. Shi, J. Yu, M. Tang, X. Huang, Fabrication of superhydrophobic surface with improved corrosion inhibition on 6061 aluminum alloy substrate, *Appl. Surf. Sci.* 342 (2015) 76–83.
- [22] P. Liu, Y. Gao, F. Wang, J. Yang, X. Yu, W. Zhang, L.u. Yang, Superhydrophobic and self-cleaning behavior of Portland cement with lotus-leaf-like microstructure, *J. Cleaner Prod.* 156 (2017) 775–785.
- [23] A. Volpe, C. Gaudioso, A. Ancona, Laser Fabrication of Anti-Icing Surfaces, *A Review. Materials* 13 (24) (2020) 5692, <https://doi.org/10.3390/ma13245692>.
- [24] P. Wan, J. Wu, LiLi Tan, B. Zhang, K.e. Yang, Research on super-hydrophobic surface of biodegradable magnesium alloys used for vascular stents, *Mater. Sci. Eng., C* 33 (5) (2013) 2885–2890.

- [25] S. Xu, et al., Fabrication of hierarchical structures on steel mesh with good superhydrophobicity and anti-corrosion property, *Colloids Surf., A* 602 (2020), 125168.
- [26] S. Li, et al., Biomimetic superhydrophobic and antibacterial stainless-steel mesh via double-potentiostatic electrodeposition and modification, *Surf. Coat. Technol.* 403 (2020), 126355.
- [27] Z. Wang, et al., Superhydrophobic nickel coatings fabricated by scanning electrodeposition on stainless steel formed by selective laser melting, *Surf. Coat. Technol.* 377 (2019), 124886.
- [28] B.o. Wu, M. Zhou, J. Li, X. Ye, G. Li, L. Cai, Superhydrophobic surfaces fabricated by microstructuring of stainless steel using a femtosecond laser, *Appl. Surf. Sci.* 256 (1) (2009) 61–66.
- [29] J.-H. Kim, A. Mirzaei, H.W. Kim, S.S. Kim, Facile fabrication of superhydrophobic surfaces from austenitic stainless steel (AISI 304) by chemical etching, *Appl. Surf. Sci.* 439 (2018) 598–604.
- [30] D. Nanda, A. Sahoo, A. Kumar, B. Bhushan, Facile approach to develop durable and reusable superhydrophobic/superoleophilic coatings for steel mesh surfaces, *J. Colloid Interface Sci.* 535 (2019) 50–57.
- [31] Zhang, H., et al., Fabrication of Super-hydrophobic Surface on Stainless Steel using Chemical Etching Method, in *Key Engineering Materials*, F. Tang, F. Tang Editors. 2013. p. 33-38.
- [32] Y. Liu, Y. Bai, J. Jin, L. Tian, Z. Han, L. Ren, Facile fabrication of biomimetic superhydrophobic surface with anti-frosting on stainless steel substrate, *Appl. Surf. Sci.* 355 (2015) 1238–1244.
- [33] Z. Zhang, et al., Preparation of intricate nanostructures on 304 stainless steel surface by SiO<sub>2</sub>-assisted HF etching for high superhydrophobicity, *Colloids Surf., A* 586 (2020), 124287.
- [34] Z. Zhang, X. Liu, D. Li, Y. Lei, T. Gao, B. Wu, J. Zhao, Y. Wang, G. Zhou, H. Yao, Mechanism of ultrasonic impregnation on porosity of activated carbons in non-cavitation and cavitation regimes, *Ultrason. Sonochem.* 51 (2019) 206–213.
- [35] A.R. Rezk H. Ahmed S. Ramesan L.Y. Yeo High Frequency Sonoprocessing: A New Field of Cavitation-Free Acoustic Materials Synthesis Processing, and Manipulation. *ADVANCED SCIENCE* 8 1 2021 2001983 10.1002/advs.v8.1 10.1002/advs.202001983.
- [36] Z. Liang, G. Zhou, S. Lin, Y. Zhang, H. Yang, Study of low-frequency ultrasonic cavitation fields based on spectral analysis technique, *Ultrasonics* 44 (1) (2006) 115–120.
- [37] H. Xu, J. Tu, F. Niu, P. Yang, Cavitation dose in an ultrasonic cleaner and its dependence on experimental parameters, *Appl. Acoust.* 101 (2016) 179–184.
- [38] T. Thanh Nguyen, Y. Asakura, S. Koda, K. Yasuda, Dependence of cavitation, chemical effect, and mechanical effect thresholds on ultrasonic frequency, *Ultrason. Sonochem.* 39 (2017) 301–306.
- [39] H.-B. Lee, P.-K. Choi, Acoustic power dependences of sonoluminescence and bubble dynamics, *Ultrason. Sonochem.* 21 (6) (2014) 2037–2043.
- [40] Y.C. Sang, A.B. Albadarin, A.H. Al-Muhtaseb, C. Mangwandi, J.N. McCracken, S.E. J. Bell, G.M. Walker, Properties of super-hydrophobic copper and stainless steel meshes: Applications in controllable water permeation and organic solvents/water separation, *Appl. Surf. Sci.* 335 (2015) 107–114.
- [41] Leonov, et al. Increasing of ultrasonic technologies efficiency and development of ultrasonic devices for industry, medicine and agriculture. 2004: IEEE.
- [42] N. Noor, et al., Resistant starch type 2 from lotus stem: Ultrasonic effect on physical and nutraceutical properties, *Ultrason. Sonochem.* 76 (2021), 105655.
- [43] D. Ramachandiran, M. Elangovan, K. Rajesh, Structural, optical, biological and photocatalytic activities of platinum nanoparticles using salixtetrasperma leaf extract via hydrothermal and ultrasonic methods, *OPTIK* 244 (2021) 167494, <https://doi.org/10.1016/j.ijleo.2021.167494>.
- [44] Khmelev, V.N., et al., Specific Features of the Realization of Ultrasonic Action in Liquid Media under Excessive Pressure. 2019 20TH INTERNATIONAL CONFERENCE OF YOUNG SPECIALISTS ON MICRO/NANOTECHNOLOGIES AND ELECTRON DEVICES (EDM 2019), 2019: p. 235-239.
- [45] J. Li, X. Bai, X. Tang, F. Zha, H. Feng, W. Qi, Underwater superoleophobic/underoil superhydrophobic corn cob coated meshes for on-demand oil/water separation, *Sep. Purif. Technol.* 195 (2018) 232–237.
- [46] R. Liu, S. Young, S. Dangwal, I. Shaik, E. Echeverria, D. McIlroy, C. Aichele, S.-J. Kim, Boron substituted MFI-type zeolite-coated mesh for oil-water separation, *Colloids Surf., A* 550 (2018) 108–114.
- [47] W.-T. Cao, Y.-J. Liu, M.-G. Ma, J.-F. Zhu, Facile preparation of robust and superhydrophobic materials for self-cleaning and oil/water separation, *Colloids Surf., A* 529 (2017) 18–25.
- [48] Z. Xu, D. Jiang, Z. Wei, J. Chen, J. Jing, Fabrication of superhydrophobic nano-aluminum films on stainless steel meshes by electrophoretic deposition for oil-water separation, *Appl. Surf. Sci.* 427 (2018) 253–261.
- [49] Z.-Y. Luo, S.-S. Lyu, Y.-X. Fu, Y.i. Heng, D.-C. Mo, The Janus effect on superhydrophilic Cu mesh decorated with Ni-NiO/Ni(OH)<sub>2</sub> core-shell nanoparticles for oil/water separation, *Appl. Surf. Sci.* 409 (2017) 431–437.
- [50] L. Zhang, Z. Gong, B. Jiang, Y. Sun, Z. Chen, X. Gao, N.a. Yang, Ni-Al layered double hydroxides (LDHs) coated superhydrophobic mesh with flower-like hierarchical structure for oil/water separation, *Appl. Surf. Sci.* 490 (2019) 145–156.
- [51] Y. Jiang, et al., Stainless-steel-net-supported superhydrophobic COF coating for oil/water separation, *J. Membr. Sci.* 587 (2019), 117177.
- [52] S.A. Khan, V. Ialyshev, V.V. Kim, M. Iqbal, H. Al Harmi, G.S. Boltaev, R.A. Ganeev, A.S. Alnaser, Expedited Transition in the Wettability Response of Metal Meshes Structured by Femtosecond Laser Pulses for Oil-Water Separation. *Frontiers in Chemistry* 8 (2020), <https://doi.org/10.3389/fchem.2020.0076810.3389/fchem.2020.00768.s00110.3389/fchem.2020.00768.s002>.
- [53] N.i. Wen, X. Miao, X. Yang, M. Long, W. Deng, Q. Zhou, W. Deng, An alternative fabrication of underoil superhydrophobic or underwater superoleophobic stainless steel meshes for oil-water separation: Originating from one-step vapor deposition of polydimethylsiloxane, *Sep. Purif. Technol.* 204 (2018) 116–126.
- [54] C. Cao, J. Cheng, Fabrication of superhydrophobic copper stearate@Fe<sub>3</sub>O<sub>4</sub> coating on stainless steel meshes by dip-coating for oil/water separation, *Surf. Coat. Technol.* 349 (2018) 296–302.
- [55] Y. Zhan, et al., Robust super-hydrophobic/super-oleophilic sandwich-like UIO-66-F4@rGO composites for efficient and multitasking oil/water separation applications, *J. Hazard. Mater.* 388 (2020), 121752.